Bull Volcanol (2017) 79:82
DOI 10.1007/s00445-017-1166-0

RESEARCH ARTICLE

Phreatic activity and hydrothermal alteration in the Valley of Desolation, Dominica, Lesser Antilles

Klaus Mayer[1] · **Bettina Scheu**[1] · **Tim I. Yilmaz**[1] · **Cristian Montanaro**[1,2] · **H. Albert Gilg**[3] · **Stefanie Rott**[1] · **Erouscilla P. Joseph**[4] · **Donald B. Dingwell**[1]

Received: 25 February 2017 / Accepted: 26 September 2017

Abstract Phreatic eruptions are possibly the most dramatic surface expressions of hydrothermal activity, and they remain poorly understood. The near absence of precursory signals makes phreatic eruptions unpredictable with respect to both time and magnitude. The Valley of Desolation (VoD), Dominica, located close to the Boiling Lake, the second largest high-temperature volcanic crater lake in the world, hosts vigorous hydrothermal activity with hot springs, mud pools, fumaroles, and steaming ground. A phreatic or phreatomagmatic eruption from this site is considered to be the most likely scenario for future volcanic activity on Dominica. Yet there is little information regarding the trigger mechanisms and eruption processes of explosive events at this active hydrothermal center, and only a very small number of studies have investigated hydrothermal activity in the VoD. We therefore conducted two field campaigns in the VoD to map hydrothermal activity and its surficial phenomena. We also investigated alteration processes and their effects on degassing and phreatic eruption processes. We collected in situ petrophysical properties of clay-rich unconsolidated samples, and together with consolidated rock samples, we investigated the range of supergene and hydrothermal alteration in the laboratory. In addition, we performed rapid decompression experiments on unconsolidated soil samples. Our results show that alteration leads to an increasing abundance of clay minerals and a decrease in both strength and permeability of the rocks. In the immediate vicinity of degassing acid-sulfate fluids, advanced argillic alteration yields a mineral zoning which is influenced by meteoric water. The water-saturated basal zone is dominated by kaolinite run 0whereas alunite formation is favored at and above the groundwater table where atmospheric oxidation of H_2S to H_2SO_4 occurs (e.g., steam-heated alteration). Alteration effects may in turn inhibit degassing at the surface, increasing the potential for pressurization in the subsurface and thus lead to phreatic eruptions. Rapid decompression experiments, together with ballistic trajectory calculations, constrain estimates of the conditions prior to the 1997 small-scale phreatic event in the VoD. The results presented here may serve as a contribution to the understanding of the hazard potential of ongoing hydrothermal activity within the VoD. On a broader perspective, our results will help evaluate hydrothermal activity in similar areas worldwide which might also have the potential for phreatic eruptions, for instance Poas (Costa Rica) or Tongariro and Waimangu (New Zealand).

Keywords Phreatic eruption · Valley of Desolation · Hydrothermal alteration · Degassing · Permeability

Editorial responsibility: P-S Ross

Electronic supplementary material The online version of this article (https://doi.org/10.1007/s00445-017-1166-0) contains supplementary material, which is available to authorized users.

✉ Klaus Mayer
klaus.mayer@min.uni-muenchen.de

✉ Cristian Montanaro
c.montanaro@auckland.ac.nz

[1] Department of Earth and Environmental Sciences, Ludwig-Maximilians-Universität München (LMU), Theresienstrasse 41/III, 80333 Munich, Germany

[2] School of Environment, University of Auckland, Auckland, New Zealand

[3] Lehrstuhl für Ingenieurgeologie, Technische Universität München, Arcisstrasse 21, 80333 Munich, Germany

[4] Seismic Research Centre, University of the West Indies, St. Augustine, Trinidad and Tobago

Published online: 10 November 2017

Introduction

Dominica, with nine distinct volcanic centers across an island area of 750 km^2, has one of the highest concentrations of potentially active volcanoes in the world (Lindsay et al. 2003). Abundant geothermal phenomena can be observed, especially across the southern part of the island. The Valley of Desolation (VoD)-Boiling Lake area is one of the most vigorous hydrothermal centers, hosting hot springs, mud pools, fumaroles, steaming ground, and the Boiling Lake. The "Boiling Lake" is the local name for one of Dominica's most popular tourist attractions, as it is the world's second largest high-temperature crater lake (Di Napoli et al. 2014). Such lakes contain mainly meteoric water with a low pH and are high temperature due to the heat transfer from fumarolic emissions of the active crater below the lake (Fournier et al. 2009).

Craters within this area have been formed as a result of phreatic and/or phreatomagmatic eruptions (Lindsay et al. 2005). Even though the island, with a population of 72,000, is not densely populated (Lindsay et al. 2005), the tourist flux of ~ 80,000 people per year is significant (World Bank 2017).

A phreatic eruption from one of these sites is considered as the most likely scenario for future volcanic activity on Dominica (Lindsay et al. 2005) representing a major threat to the resident and visiting populations and especially to people in close proximity to the sites. Hazards associated with such eruptions include ballistics, surges, and jets of mud and rocks without any juvenile components (Montanaro et al. 2016). The absence of any precursory signals (Browne and Lawless 2001) further increases the hazard potential of such eruptions from the VoD (as seen in many other phreatic events worldwide). Phreatic and phreatomagmatic eruptions are well-researched problems of high concern not only in the active hydrothermal systems of a small volcano island (e.g., Gurioli et al. 2012) but also in densely populated urban areas (e.g., Mayer et al. 2016). This is accentuated by the fact that explosive activity can be triggered suddenly and, at any time, to impinge on the immediate population with little or no warning.

Relatively little information is available for the Valley of Desolation-Boiling Lake system; exceptions being the studies of Fournier et al. (2009), Joseph et al. (2011), Smith et al. (2013), and Di Napoli et al. (2014). Regarding historic phreatic events, the literature is limited to the nineteenth century studies of Nicholls (1880), Watt (1880), and Sapper (1903), plus those of James (1997) and Lindsay et al. (2005). In the past, studies have focused on the geology of the island and provided some geological descriptions in the context of volcanic hazard assessment (Lindsay et al. 2005). Joseph et al. (2011) investigated the geochemistry of the main geothermal areas, including the Valley of Desolation-Boiling Lake system. Further studies have been conducted on the Boiling Lake with respect to episodic drainage events (Fournier et al. 2009; Di Napoli et al. 2014). The last drainage occurred in December 2016 and was accompanied by a small mud-rich explosion.

Despite the abundance of surficial hydrothermal expressions within the Valley of Desolation-Boiling Lake area (Joseph et al. 2011), no modern detailed descriptions or geological maps exist. Although soil properties, as affected by weathering processes, across the island have been investigated by Rouse et al. (1986) and Rao (1996), detailed descriptions of supergene alteration—mainly due to oxidation and chemical weathering in the presence of cool meteoric waters or hydrothermal alteration—i.e., changes resulting from the interaction with high-temperature aqueous fluids (Pirajno 2009) within the Valley of Desolation, and their influences on degassing, are still lacking. Although the wide range of initial pressures, temperatures, and the proportion of liquid water within the decompressing fluid, as well as the different rock types that characterize the Valley of Desolation, can result in phreatic eruptions with variable degrees of explosivity (Browne and Lawless 2001; Montanaro et al. 2016), there is also little information regarding the triggering mechanisms and eruption processes for the eruptions that have occurred in historic times. Hydrothermal alteration of the host rocks, or of the ejecta generated by the historic eruptions, has only been briefly described by James (1997) and Lindsay et al. (2005).

Thus to understand the effects of hydrothermal alteration, we carried out field and laboratory measurements on rocks from the Valley of Desolation crater. In particular, the effects on the geochemical and mineralogical composition of the rocks, as well as on their properties (including in situ permeability, porosity, and strength), and thus on the surficial, hydrothermal activity, were assessed. Rapid decompression experiments allowed us to investigate the ejection behavior of the hydrothermally altered, unconsolidated material collected from the vicinity of the last phreatic eruption in 1997. Our results allowed us to characterize the type and intensity of hydrothermal alteration within the Valley of Desolation and shed light to the processes leading to its last eruptive event.

Geological setting

The island of Dominica is part of the Lesser Antilles (Fig. 1), a volcanic arc formed by the subduction of the North and South American plates below the Caribbean plate at a rate of 2.0 cm/year (Smith et al. 2013). With ~ 40 km^3 of erupted magma within the past 100 ka, Dominica has the highest erupted magma volume of all the Lesser Antilles volcanic islands over this period (Di Napoli et al. 2014). Dominica has a rugged topography covered by dense tropical vegetation (Lindsay et al. 2005). Geologically, the island consists almost entirely of volcanic rocks and their weathering products, with the exception of some minor Pleistocene conglomerates and limestones (Lindsay et al. 2005). Due to the tropical climate with a

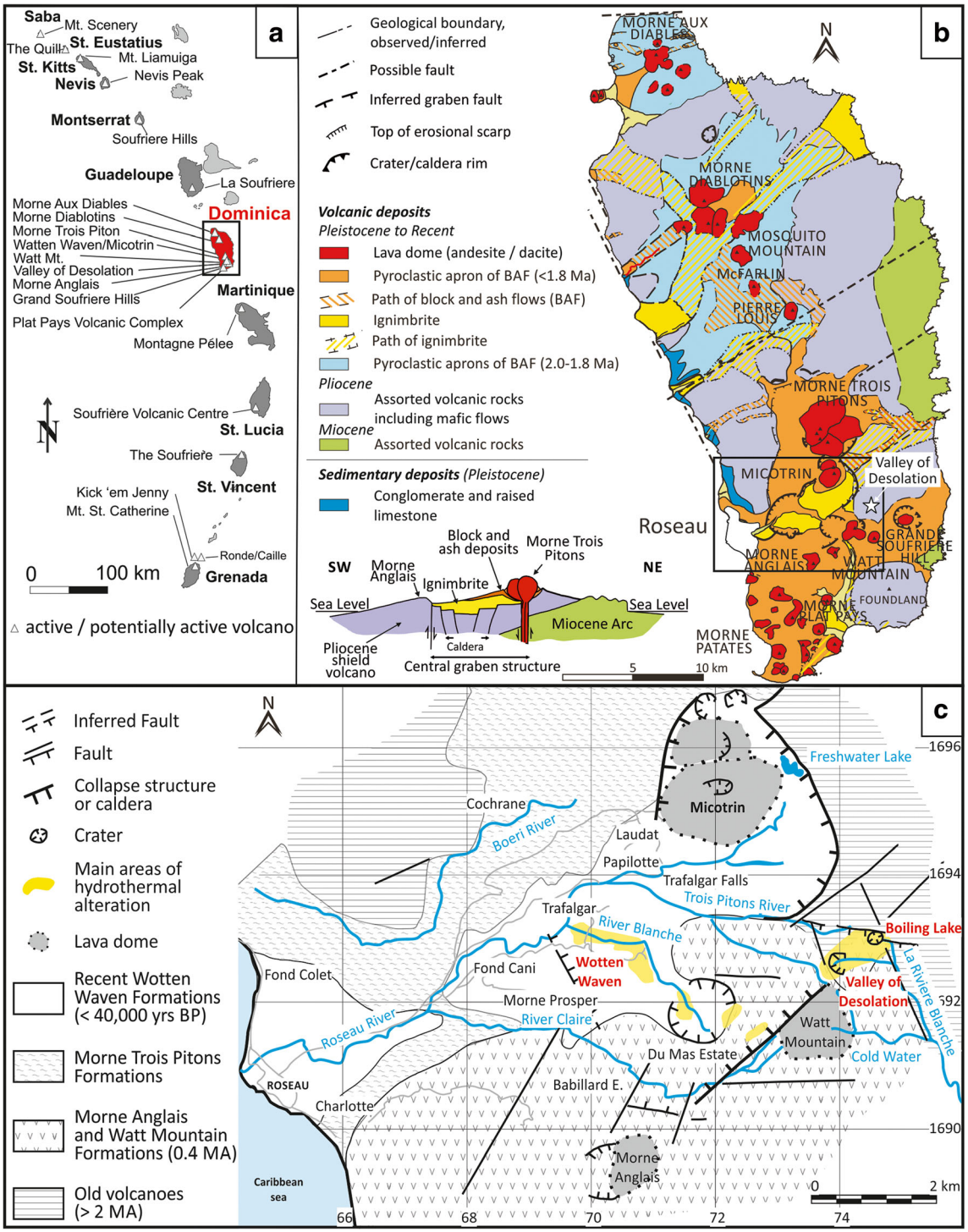

Fig. 1 **a** Simplified geographical map of the Lesser Antilles showing the location of Dominica. Modified after Joseph et al. (2011). **b** Simplified geological map of Dominica. Modified after Roobol and Smith (2004). **c** Simplified geological map of the Roseau Valley showing faults, inferred faults, collapse structures or calderas, craters, lava domes, and the main areas of hydrothermal activity. Modified after Traineau et al. (2015)

high annual rainfall (3000 mm/year) and the heavily-incised topography in which slopes frequently exceed an angle of 40°, the island is subject to extreme weathering and physical denudation, mainly involving mass-movement phenomena (Rouse et al. 1986; Rad et al. 2013). The predominantly andesitic-dacitic volcanic products make up lava domes, block-and-ash flows and ignimbrites (Roobol and Smith 2004; Lindsay et al. 2005) (Fig. 1b), with the oldest igneous rocks being dated to Miocene times (7 Ma; Demange et al. 1985). About 1.6 Ma ago, volcanic activity migrated from the north to the

south of the island (Lindsay et al. 2005). However, based on seismic activity, Morne Diablotin and Morne aux Diables (located in the north of the island) still show potential for further activity (Joseph et al. 2011). Since the late Pleistocene, seven major andesitic-dacitic subduction-related volcanic centers, associated with geothermal systems, have been active in the southern part of Dominica (Lindsay et al. 2003). Most of them have erupted within the last 10 ka (Lindsay et al. 2005; Joseph et al. 2011).

The Valley of Desolation (VoD) is situated within the Morne Trois Pitons National Park in the south-central part of Dominica and represents a phreatic or phreatomagmatic eruption crater within massive lavas associated with the Peléan dome of Morne Watt (Fig. 1; Traineau et al. 2015). According to Traineau et al. (2015), the VoD and the nearby Boling Lake crater are related to a local fault system trending NE–SW and NNW–SSE (Fig. 1c). Since their formation, block-and-ash flow deposits, as well as landslide debris derived from the surrounding slopes, have partially filled the VoD (Lindsay et al. 2005).

Today, the VoD-Boiling Lake area is one of Dominica's main geothermally active areas (Joseph et al. 2011). However, the details of its geothermal evolution remain unclear, despite the presence of several small, crater-shaped depressions associated with hydrothermal activity within the area. What is known is that dilution of acidic gases in near surface oxygenated groundwater currently leads to the discharge of predominantly acid-sulfate fluids with variable sulfate concentration (100–4200 ppm) and moderate-to-high acidity with a pH of ≤ 4 (Joseph et al. 2011).

Holocene and recent eruption record

Phreatic eruptions have occurred in the VoD-Boiling Lake area since at least 4000 years ago (Lindsay et al. 2005). According to Demange et al. (1985), the oldest eruptions in the area occurred ~ 4050 years ago, but no details about the vent location are available. Two other prehistoric eruptions (~ 3750 and ~ 2900 years ago) are believed to have generated small explosion craters within the VoD-Boiling Lake area (Demange et al. 1985; Lindsay et al. 2005). The formation of Boiling Lake itself (undated) may have resulted from one of these two more recent events (Fournier et al. 2009).

According to Nicholls (1880), Watt (1880), Sapper (1903), and Lindsay et al. (2005), the first historic explosive event from the VoD-Boiling Lake area occurred on January 4, 1880. However, Robson and Willmore (1955) found an earlier eruption which occurred in 1863, in the Eastern Hot Springs area (Fig. 2a, b). The well-documented 1880 event was speculated to have been associated with a decrease in barometric pressure during heavy rainfall by Nicholls (1880). Nicholls (1880) suggested an eruption from a hydrothermally active crater, which showed solfataric activity prior to the event. The 1880 eruption created ash fall over an area of at least 50 km^2 and extending westward to a distance of 19 km, covering the city of Roseau with a few millimeters of ash (Nicholls 1880). This steam driven phreatic eruption ejected juvenile-free tephra, consisting of mineral fragments and altered material (Wadsworth 1880). Within and beyond the crater edge, trees were destroyed by ballistics and the ground was covered by meter-sized debris (Nicholls 1880). Endlich (1880) estimated a total volume of 27 million tons for this eruption, which generated a WSW–ENE elongated, ~ 180-m-deep, ovoid crater breached to the NE. These dimensions correspond well to the topography of the Valley today (Fig. 2c, d).

Sapper (1903) visited and investigated the VoD-Boiling Lake area in 1903, mapped the hydrothermal features, and made temperature measurements within three distinct craters. His map, given in Fig. 2a, shows the Boiling Lake located within the easternmost crater, a second crater characterized by fumarolic activity but with signs of vegetation regrowth along the crater walls, and a third crater, the VoD—formerly known as Grande Soufrière (Sapper 1903). This depression was slightly inclined towards the northeast, and was free of vegetation (Sapper 1903). Despite ascribing the strongest hydrothermal activity of the investigated area to the VoD, Sapper (1903) did not consider it to be the location of the 1880 eruption. This stands in contrast to field observations made just days after the eruption, which clearly confirm the VoD as being the source location (Endlich 1880; Nicholls 1880). Documented reports of the activity in the area following the 1880 eruption are rare.

A phreatic event occurred on July 8–9, 1997, during a tropical storm associated with heavy rain. This unwitnessed eruption, which involved just a few tons of erupted material, was significantly smaller in magnitude than the 1880 eruption (James 1997). It was suggested to have been triggered by a landslide, which might have happened on the day of, or in the days preceding, the eruption (James 1997). The burial of the fumarolic vents by the landslide deposits (which were 2.5–3 m thick; James 2013, personal communication) would have hindered fumarolic emissions. This led to pressurization of the hydrothermal system and ultimately resulted in this small-volume phreatic eruption (James 1997). According to observations made by James (1997) on July 13, a 2.5- to 7.5-m-deep and 19-m-long eruption crater, which contained a bubbling mud pool, was superseded by a valley (Fig. 2e). This gully-like feature named "Mini valley" was formed by erosion of the loose material within the eruption crater by surface runoff (James 1997). At least eight fumaroles and a hot spring at 85 °C developed within the "Mini valley" (James 1997). Mud, pebbles, and sulfur-bearing fragments of rock were found asymmetrically distributed around the "Mini valley" with the deposit extending 53 m to the west (James 1997), due to the prevailing wind direction being westerly (Fig. 2f).

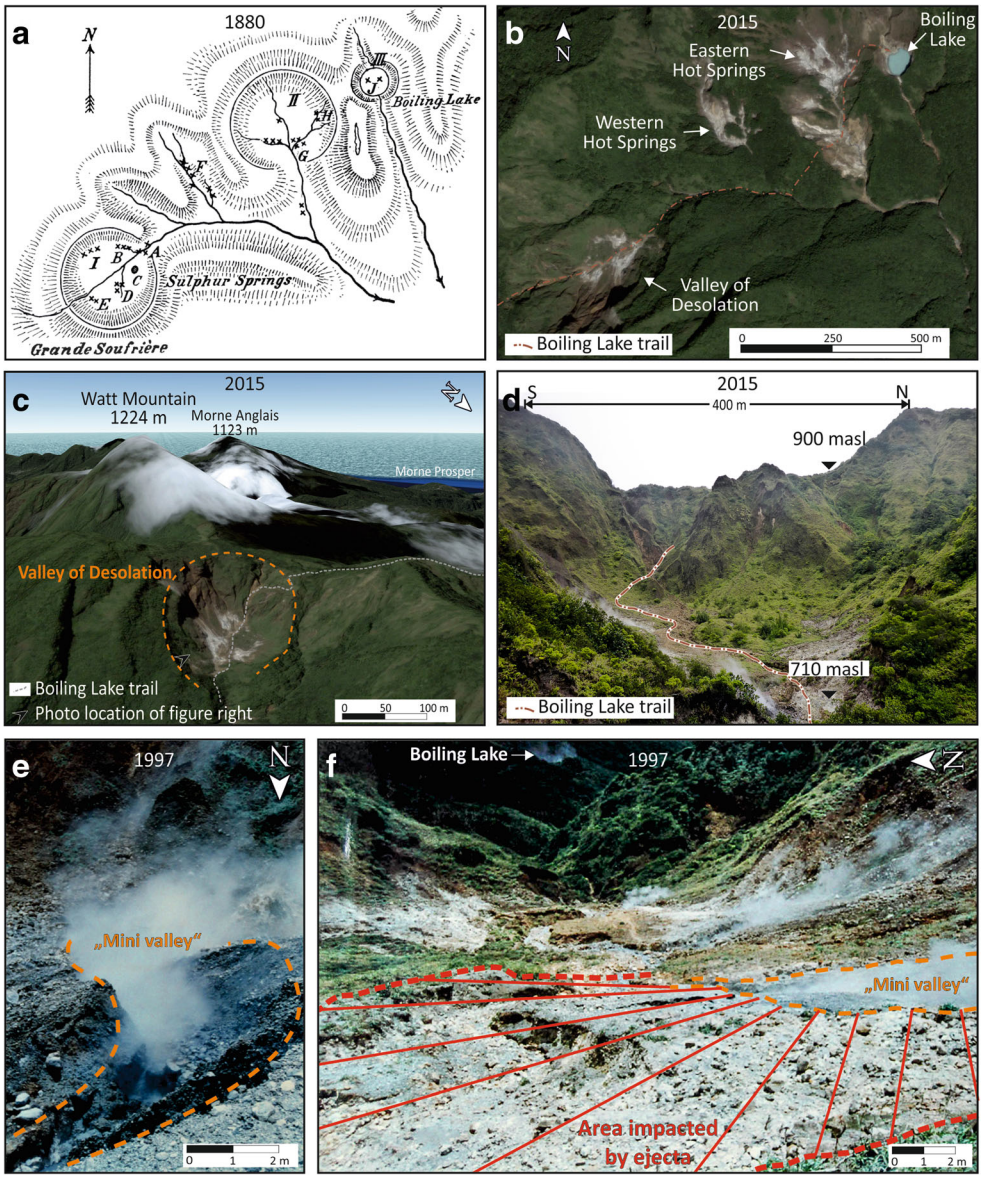

Fig. 2 **a** Topographic and hydrothermal activity map of the Valley of Desolation-Boiling Lake area indicating morphological craters [I, II, III] and hydrothermal features. The features indicated on the map are: [*A*] steaming, bubbling hot spring (92 °C) and highly spraying mineral spring, [*B*] strongly steaming fumaroles (96 °C) surrounded by sulfur precipitations and several small fumaroles along the northern crater margin, [*C*] bubbling and spraying mud pools (max. 7 m diameter; 84 °C), [*D*] spraying fumaroles (2 m high; 94.5 °C), [*E*] several small fumaroles and hot springs (92 °C), [*F*] strong fumaroles and several hot springs (max. 95 °C), [*G*] vigorously bubbling hot spring (80 °C) and several other springs, and [*H*] two springs (40.5 and 42 °C). Modified after Sapper (1903). **b** Recent Google Earth™ image showing the same area in 2015. Note the striking similarities between the hand drawn map and the satellite image. **c** Google Earth™ image (2015) showing the outline of the Valley of Desolation (dashed line), the suggested location of the phreatic eruption of January 4, 1880. **d** Photograph of the Valley of Desolation (2015) surrounded by steep slopes. The Boiling Lake trail (dash-dotted line) enters the valley in the west, passes by the hydrothermal phenomena and exits at the lowest point in the east. **e**, **f** Photographs taken by A. James ~ 5 weeks after the 1997 phreatic eruption in the Valley of Desolation. **e** Following the eruption, the crater was affected by erosion of surficial runoff, which changed its shape and created a gully-like "Mini valley" surrounded by loose phreatic debris. **f** Distribution of ejecta mainly in a sector from the north to the south-southwest of the vent location

Since this event, the VoD has exhibited vigorous hydrothermal activity. The activity of the fumaroles and the discharge of the springs show fluctuations possibly affected by rainfall and landslides, but without significant variations in chemistry (Jeffrey 2013, personal communication; Joseph et al. 2011). The volcanic rocks of the area are exposed to ongoing weathering and hydrothermal alteration (Lindsay et al. 2005). Subsequent to the 1997 eruption, a seismic station was installed on Morne Nicholls by the University of West Indies (UWI) Seismic Research Centre to monitor seismic activity in the VoD-

Boiling Lake area (James 1997). Regular geothermal monitoring was also initiated in November 2000 by the UWI. This includes full gas and water chemistry analyses on an annual basis for investigation of compositional variations related to changing volcanic activity (Joseph et al. 2011).

Methodology

Two field campaigns were conducted in April 2013 and May 2015 to study the hydrothermal activity, its alteration effects and processes controlling the degassing within the VoD. Petrophysical and soil mechanical properties were determined in the field and in the laboratory, and these were compared with the mineralogical and geochemical compositions of the rocks. Further laboratory investigation allowed study of the behavior of selected samples during rapid decompression.

Mapping and sampling

Hydrothermal features, as well as surficial lithological units, within the VoD were mapped. Rocks in the vicinity of hydrothermal phenomena are the most intensely altered, showing clear signs of changes concerning their rock properties, particularly mineralogy, porosity, permeability, and strength, as is well-known at the hydrothermal systems of Campi Flegrei, Vulcano, White Island, and many others (Pola et al. 2012, Mayer et al. 2015, Gurioli et al. 2012, Heap et al. 2017). We collected rock and soil samples affected by supergene and hydrothermal alteration at three different locations within the VoD and measured in situ sample properties of soil samples.

A recent landslide in the east of the valley created an outcrop (S1) which yielded access for sampling of the moderately weathered parent rock and altered equivalents (Figs. 5 and 6). A second landslide on the northern slope also enabled sampling of the in situ parent rock and the secondary supergene alteration (S2). Both locations showed similar changes in macroscopic texture and rock/soil color due to effects of alteration, being characterized by a transition from gray, weakly altered, andesitic parent rock (VoD1, VoD2), to moderately altered clay-dominated horizons (VoD3, VoD4). Two further types of alteration products were investigated and sampled close to F1 within the "Mini valley" (S3) where a 2-m-deep escarpment comprises a lower section of a clay-rich, homogeneous, blue-gray layer (VoD5), overlain by a white, heterogeneous, and partly loose, breccia-like material (VoD6). To account for heterogeneities, both horizons were sampled at three locations along the escarpment.

Cylinders used for collection and measurements of soil samples were weighed and immediately sealed for transport. This technique allowed non-destructive sampling and preservation of the sample required for investigation of additional properties (i.e., porosity, water content, and mineralogical composition) in the laboratory, which are described below.

Field-based characterization

A PL-300 soil permeameter (Umwelt-Geräte-Technik) was used to measure permeability and moisture content of unconsolidated material (see Fig. S2 in the Supplementary material). Measurements were made using stainless steel cylinders (length = 61 mm; diameter = 72 mm) to extract the sample material by vertical plunging into the soil to a depth of 10 cm and finally connecting those cylinders, completely full and cleaned at both ends, to the permeameter. Air permeability was obtained within a measurement range of 5.6×10^{-16} to 6.5×10^{-13} m^2. The device determines gas volume flow through the samples connected pore network based on Darcy's law. An internal vacuum pump produces the inflow of ambient air through the soil sample, which is controlled by a valve of calibrated permeability within the apparatus. The pressure difference across the soil sample is recorded by a sensor, which provides the pressure gradient over the sampled distance. A comparison of the pressure gradient, with respect to the gradient over the calibrated section, enables the air volume flow through the soil sample to be determined and consequently its permeability. At each site, three individual soil samples were taken with the sampling cylinder and connected to the soil permeameter for measurement, to account for sample heterogeneities.

The derived air permeability characterizes the water-free pore space of the soil sample so that any variation is a function of the water content (Makó et al. 2009; Umwelt-Geräte-Technik 2012). The soil sample's moisture content was also indirectly obtained using a sensor consisting of two stainless steel rods (length = 10 cm) that measure the dielectric constant. The rods were inserted directly into the soil next to the extracted sample. Comparing the measured dielectric value with calibrated standards of pure water and dry soil yields the calculated moisture content. Field characterization further involved two handheld devices applied in soil science: (1) a pocket penetrometer which measures unconfined compressive strength (Zimbone et al. 1996) and (2) a torvain which measures undrained shear (Farquhar 2001). Volume, total weight, and cylinder weight were used to calculate bulk density of samples prior to samples being sent back.

Laboratory-based characterization

Collected soil and rock samples were analyzed in the laboratory, to determine their physical properties such as porosity, water content, and permeability (of the collected consolidated rocks). Consolidated rock samples were cored (length = 60 mm; diameter = 25 mm), with their end faces ground flat, and dried in an oven at 65 °C for at least 24 h

until fully dried following the standard procedure described by Heap et al. (2017). The same drying conditions were applied to unconsolidated samples. Dried sample powders were used for powder density measurements and mineralogical and geochemical analyses. Samples were weighed prior to and after drying to determine their water content. Powder density and volume of all cored samples were measured using a helium pycnometer (Ultrapyc 1200e®, Quantachrome) following Heap et al. (2017). This allowed determination of the connected porosity, which is a key parameter controlling rock mechanical behavior (e.g., Pola et al. 2012, Heap et al. 2017, Mayer et al. 2016). For unconsolidated samples, the dry density and water content were used to calculate the initial connected porosity within the sampling cylinder of known volume.

Gas permeability of the dried cored samples was obtained using a benchtop (nitrogen) permeameter under a confining pressure of 1 MPa to preclude fluid (nitrogen) flow around the sides of the sample. The device measures confining pressure and gas volume flux using a pressure sensor and a precision gas flow meter under several pressure gradients. This yielded permeability using Darcy's law.

Mineralogical and geochemical characterization

Bulk geochemical, as well as the mineralogical composition of each sample, was determined by wavelength dispersive X-ray fluorescence (WD-XRF) and quantitative X-ray powder diffraction (XRD) analysis on bulk samples. Details of sample preparation and analysis are reported in Appendix A1 of the Supplementary material. Geochemical analysis was further employed to determine the type and degree of alteration. The relationship between chemical changes and alteration was evaluated using five indices, as proposed for characterization of the degree of alteration in different lithologies (see Pola et al. 2012 and references therein). These indices, which are based on the weight percent ratio of major elements, assume that distribution of chemical elements is controlled by the degree of alteration (Duzgoren-Aydin et al. 2002).

Rapid decompression experiments

Unconsolidated samples, collected from the escarpment of the "Mini valley," were used for rapid decompression experiments to investigate the ejection behavior of heavily altered, clay-rich material. Details of the general procedure and specifications of the experimental setup are reported in Appendix A2 of the Supplementary material. Samples were carefully placed into sample holders to ensure preservation of sample texture and water content and then mounted into the autoclave. Experimental conditions were chosen to best mimic steam-flashing during rapid decompression, close to the overpressure and temperature at which steam-flashing occurs (i.e., 0.4 MPa and 120 °C); these are the values estimated to have been associated with the phreatic eruption at VoD in 1997. Such conditions are reported to be the major trigger for this type of eruption in many other cases worldwide (Browne and Lawless 2001). Based on (1) the ejecta distribution of James (1997), (2) the thickness of the landslide deposit burying the fumarolic vents (see the "Holocene and recent eruption record" section), and (3) the temperature measurements of hydrothermal features made by Sapper (1903) and Joseph et al. (2011), two sets of experiments were run at 115 °C/0.3 MPa and 125 °C/0.5 MPa, respectively. For both conditions, the small decompression (0.3–0.5 MPa) resulted in the sudden expansion of heated liquid water flashing to steam (James 1997). Accumulation of steam and gas below a low permeability cover can also be considered to lift the overlying material and may cause fractures for degassing, as, for example, at Campi Flegrei. But taking both the distribution of ejecta and the size of the area affected by the eruption into account, this scenario is inferred to be not energetic enough and therefore unrealistic. Indeed, given the low pressures and temperatures, the simple expansion of steam and gas would not release the energy required to cause the distribution of ejecta as reported (James 1997). To account for sample heterogeneities, at least three repeats for each investigated condition and sample were performed.

Analysis of high-speed video recordings allowed the determination of particle ejection velocity. The experimental setup was equipped with LED lights facing towards the high-speed camera: see Fig. S1 of the Supplementary material to facilitate the tracking of very fine particles ejected within the gas-steam-particle mixture. Tracked particles were grouped by size into ash (< 2 mm) and lapilli (> 2 mm) and investigated individually.

Ballistic trajectory estimations

To estimate the ejection dynamics during a phreatic event similar to the 1997 eruption in the VoD, theoretical ballistic trajectory distances were calculated. For this approach, phreatic ejecta were treated as ballistic projectiles (Mastin 1995). Ejection velocity and particle size, which were obtained by high-speed video analysis, as well as particle density as determined during the rock physical characterization, were used as input parameters. The ballistic trajectories were then calculated using the Eject! software of Mastin (2001). By assuming a spherical particle shape and an ejection angle of 45°, maximum trajectory distances could be estimated. Additional information concerning the Eject! software is provided by Mastin (2001). Calculations allowed us to analyze the influence of particle size and sample type of both ash (1–2 mm) and lapilli (2–10 mm) from VoD5 and VoD6 (collected at sampling site S3) on their trajectory distances.

Results

Field results

The locations of hydrothermal features (hot springs, mud pools, and fumaroles) within the VoD are located in the geomorphological map of Fig. 3. This map also illustrates areas where the soil is affected by hydrothermal alteration, secondary precipitations, or surficial sulfur-rich encrustations. We can also see that large areas within the valley are covered by landslide debris and runoff deposits or are covered by dense vegetation. Denudation and erosion processes remove and transport most of the altered material into the valley where, in the vicinity of hydrothermal vents, these reworked rocks and soils experience further alteration due to hydrothermal activity.

Most of the fluids discharge along the southern margin of the valley. A massive landslide deposit several meters in thickness is the result of many individual events, all originating from Morne Watt in the south (Fig. 3). The lobe of the landslide deposit separates the hydrothermally active areas containing fumarole 1 (F1) from that containing fumarole 2 (F2) (Fig. 3). Each fumarole is situated within a gully that is up to 3 m deep, several meters wide, and more than 40 m long. Fumarole 3 (F3; Fig. 4b) is associated with a hot spring around which mineralization has occurred (MHS in Fig. 3), rich in silica sinter deposits. Sulfur-rich encrustations appear predominantly along gullies where the main degassing occurs (Fig. 3). Below these encrusted areas, alteration and erosion lead, occasionally, to the formation of cavities, which are unstable and have the potential to collapse easily.

Several mud pools located in the lower part of the valley showed signs of recent mud eruptions. The resulting ejecta reached the Boiling Lake trail several meters away (Fig. 4c, d).

Geochemical quantification of alteration

The indices used to estimate the degree of alteration assume immobility of aluminum and should therefore be carefully applied to heterogeneous samples, especially in environments of hydrothermal alteration (Arıkan et al. 2007; Pola et al. 2012). Nevertheless, our values for the indices correlate well with the increase in clay minerals observed in the investigated samples. CIA (Chemical Index of Alteration), PIA (Plagioclase Index of Alteration), and CIW (Chemical Index of Weathering) values generally rise due to the loss of mobile cations within facies with supergene and hydrothermal alteration. By contrast, the SA value decreases with alteration as it is reflecting the loss of silica. Further information concerning the definition of individual indices used (Table 2) is given in the Supplementary material. The loss on ignition not only correlates with the amount of clay minerals (Arıkan et al. 2007) but also shows a large increase due to the presence of alunite formed by hydrothermal alteration.

Mineralogical composition

Besides the two lithologies consisting of consolidated rocks (VoD1 and VoD2), we found four different types of soil samples (Figs. 5 and 6; Table 1). VoD1–VoD4 represents a sequence which shows an increasing degree of supergene alteration. Accordingly, the clay content increases from VoD1 to VoD4 (Table 1). Following re-deposition and exposure to sulfur-bearing, acidic fluids (Joseph et al. 2011), the rocks (VoD1–VoD4) are variably affected by intermediate argillic alteration which leads to the formation of VoD5 and VoD6.

VoD1 is a dense volcanic rock with a porphyritic texture. It mainly consists of euhedral plagioclase and sanidine as well as colloform-banded amorphous silica (opal-C) precipitated within the pore spaces (Fig. 7a). It contains minor amounts of quartz phenocrysts, euhedral pyrite, and hornblende. A significant amount of smectite, as detected by XRD analysis, confirms the alteration of feldspars (Glasmann 1982).

VoD2 is very similar in composition to VoD1 but, due to an increased degree of alteration, this sample has a higher amount of montmorillonite and a correspondingly lower proportion of sanidine and plagioclase. Core and zonal textures are caused by the replacement of sanidine by montmorillonite which leads to the occurrence of 10–30-μm-wide residual rims (Fig. 7b).

VoD3 represents the product of progressive supergene alteration and disaggregation towards the surface. This hard-packed horizon, more than 40 cm in thickness (Fig. 5), shows an increased amount of montmorillonite due to the replacement of plagioclase, sanidine, and hornblende.

VoD4 is a surficial, yellow-brown horizon with a thickness of < 20 cm. It is completely disaggregated and affected by supergene alteration, which results in an increased amount of montmorillonite. In agreement with the chemical alteration indices (Table 2), which represent the depletion of mobile alkali elements relative to immobile elements (e.g., aluminum), the degree of argillic alteration increases towards the surface.

VoD5 is a blue-gray, clay-rich layer with an outcrop thickness of ~ 1.5 m which locally contains remnants of less-altered parent rock. Acid-sulfate fluids caused leaching and the complete alteration of feldspars mainly to kaolinite, alunite, and amorphous silica. The latter are characterized by pseudomorph replacement (Fig. 7c).

VoD6 represents the upper part of the valley wall and is mainly made up of a white, breccia-like horizon (Figs. 5 and 6) consisting of altered, sub-rounded pebble-sized clasts, which are embedded in a finer-grained matrix. Some of these clasts comprise a similar andesitic composition as VoD1 and VoD2, confirming their origin as these lithologies. VoD6 consists of fine-grained (< 5 μm) alunite, a lesser amount of kaolinite, and fragments of minerals replaced by amorphous silica (Fig. 7d).

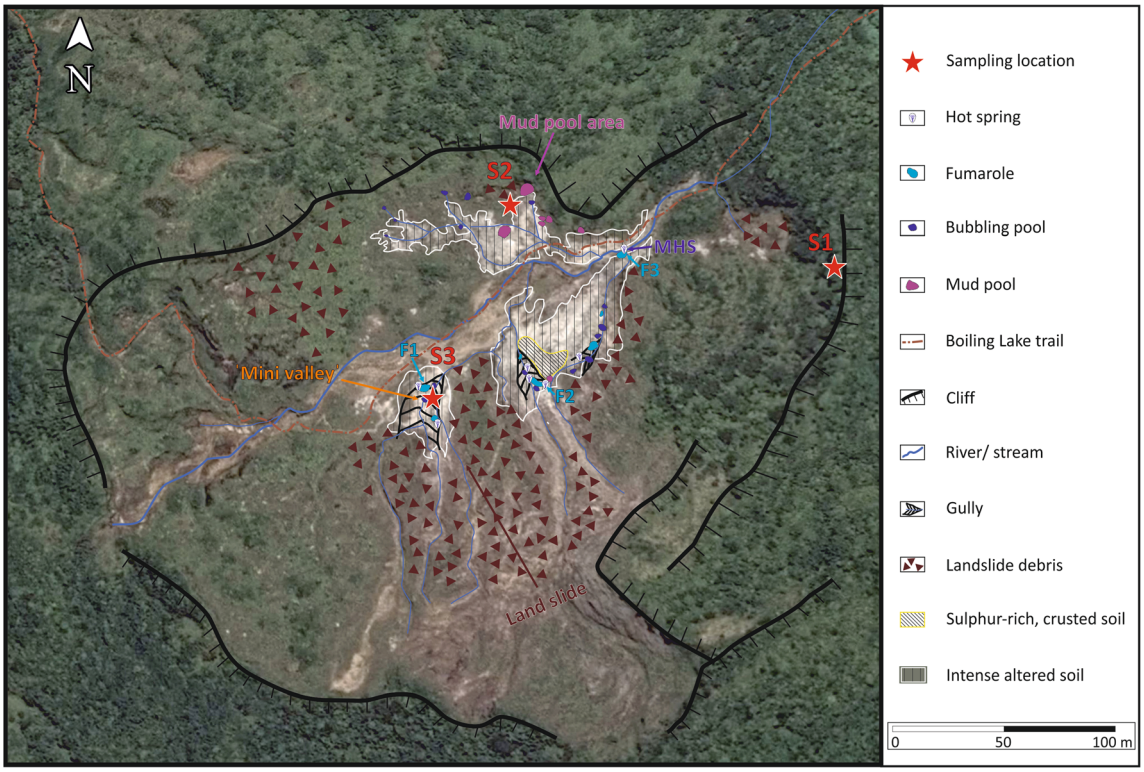

Fig. 3 Map of the Valley of Desolation (Google Earth™ image; 2015) showing the distribution of surficial hydrothermal features and main degassing sites during fieldwork in May 2015. The features marked on the map are as follows: [S1] sampling location 1, [S2] sampling location 2, [S3] sampling location 3, [F1] fumarole 1, [F2] fumarole 2, [F3] fumarole 3, [MHS] mineralized hot spring

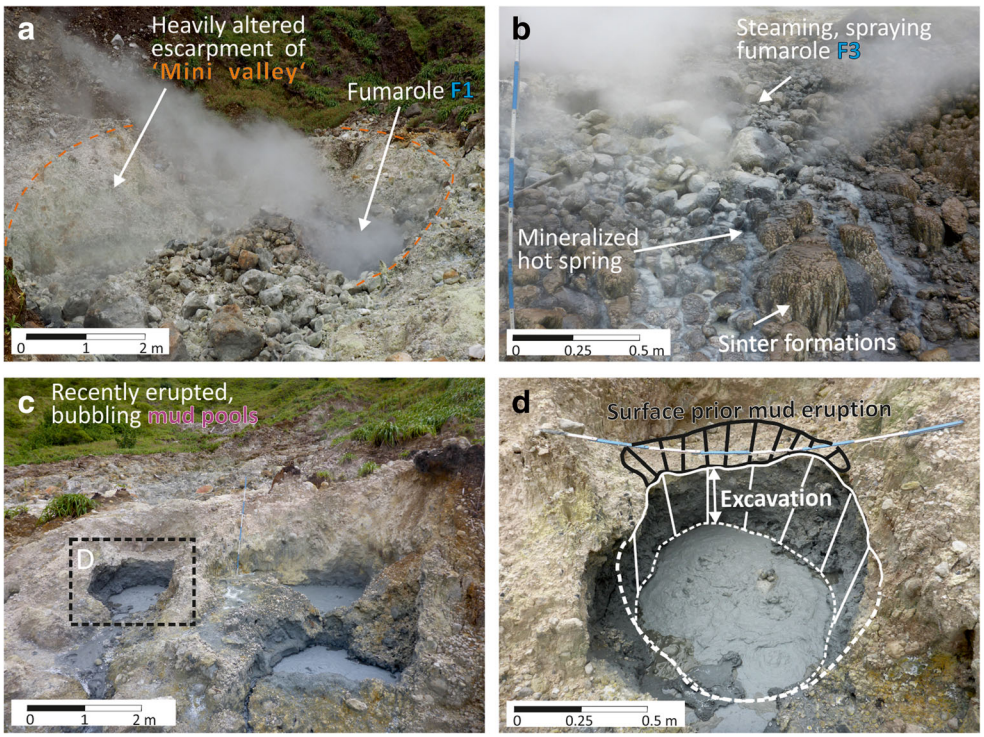

Fig. 4 Photographs of hydrothermal features from the Valley of Desolation. **a** Fumarole F1 within the "Mini valley" emitting gas. **b** Fumarole F3 and mineralized hot spring showing steam emission and sinter formation. **c** Hot bubbling mud pools showing clear signs of activity (the rectangular dashed box corresponds to the close-up displayed in **d**. **d** Close-up photograph of the recently erupted mud pool characterized by a burst which excavated approx. 0.5 m of weakly consolidated material

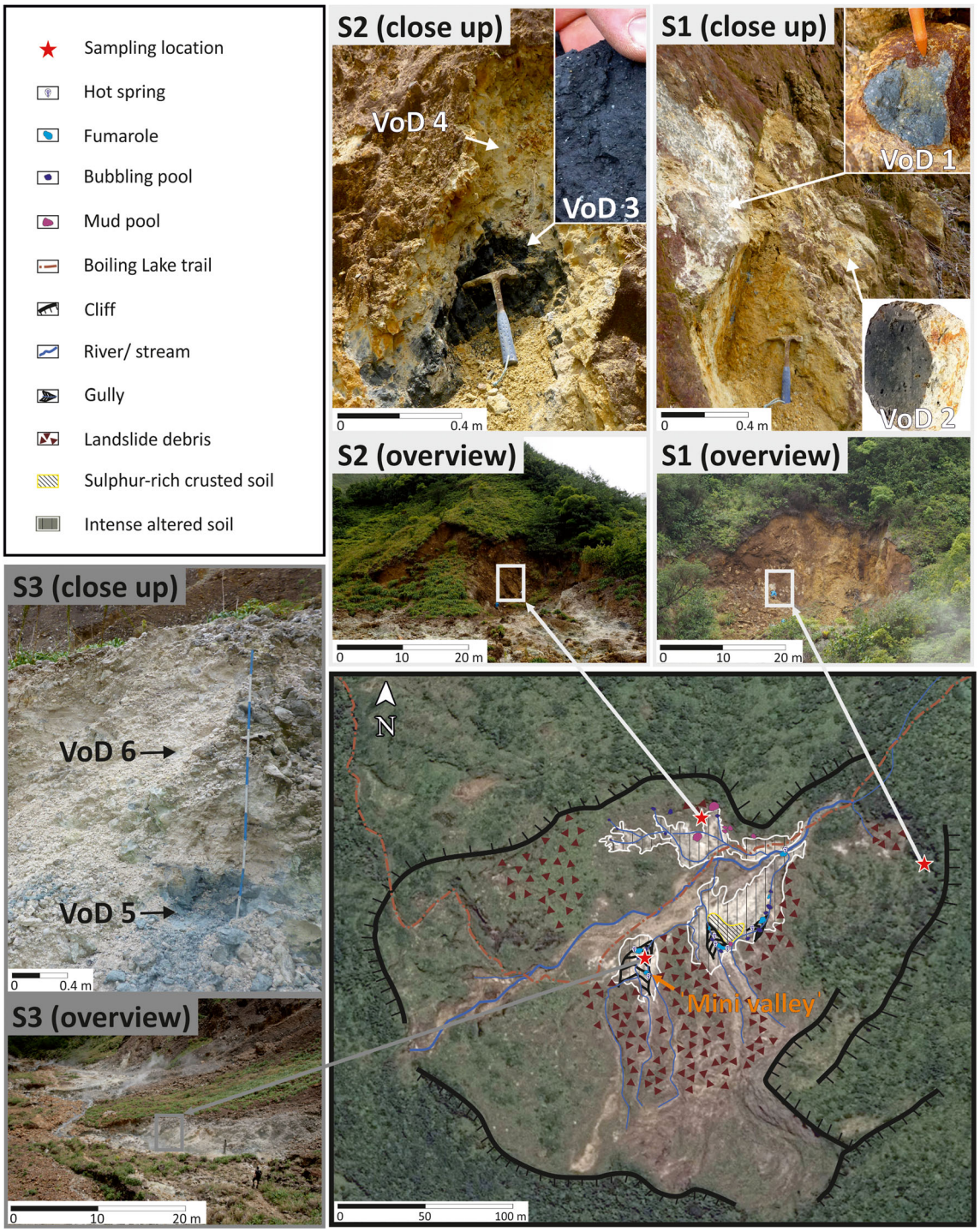

Fig. 5 Fig. S2: Map, overview, and close-up photographs showing the sampling locations within the Valley of Desolation. Sampling locations S1 and S2 were accessible due to recent landslides, which exposed consolidated and unconsolidated rocks affected by supergene alteration. Sampling location S3 represented by the escarpment within the "Mini valley" comprised two units of unconsolidated material affected by hydrothermal alteration in the close proximity of degassing vents. Corresponding close-up photographs show the alteration sequence from VoD 1 to VoD 2, from VoD 3 to VoD 4, and from VoD 5 to VoD 6, respectively

Petrophysical properties

Physical and mechanical properties of the samples as determined in the field and the laboratory are given in Table 2. In situ moisture content of unconsolidated samples ranged from 34.9 to 87.8% and was higher than the water content determined in the laboratory by drying (26.3–67.3%). The differences probably originate from

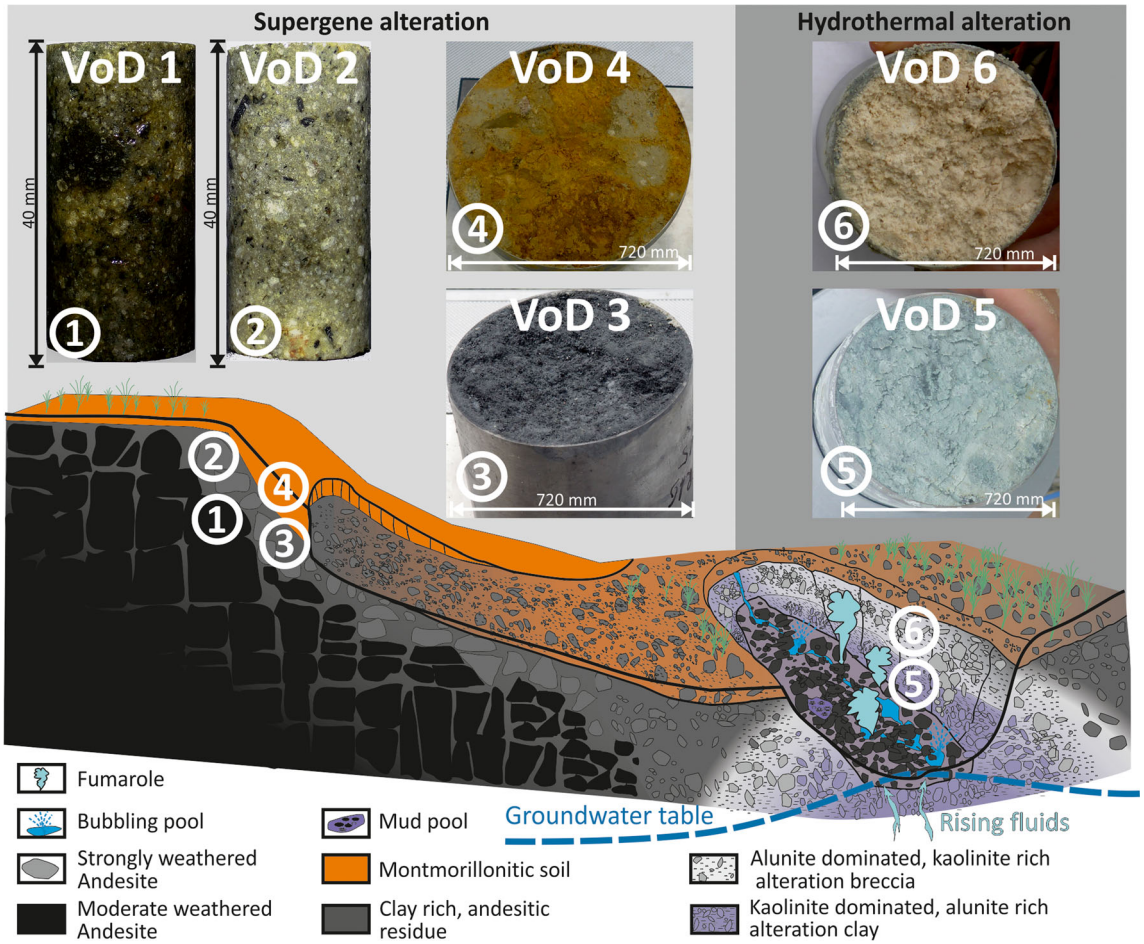

Fig. 6 Conceptual model of the origin and deposition processes of the investigated rocks as well as photographs of samples. VoD 1 to VoD 4 represent a sequence from solid to unconsolidated rocks affected by supergene argillic alteration. The progressive decomposition of feldspars results in an increased amount of montmorillonite towards the surface. In the vicinity of hydrothermal vents emitting acid sulfate fluids, rocks are affected by advanced argillic alteration. VoD 5 is dominated by kaolinite whereas VoD 6, showing a lesser degree of alteration, consists predominantly of alunite

sample heterogeneities and the loss of water during sample shipping, where samples were exposed to significant temperature and pressure changes during transport, which likely induced changes in the water distribution within the sample cylinders.

Bulk and matrix density ranges from 1.52–1.74 and 2.56–2.76 g/cm^3 for unconsolidated samples and from 2.18–2.22 and 2.49–2.61 g/cm^3 for solid rocks. The permeability results of Table 2 are the average for three measurements on each sample and range from 2.5×10^{-15} to 2.1×10^{-14} m^2. Finally, UCS (uniaxial compressive strength) and shear strength of investigated samples varies between 0.9–2.4 and 0.8–3.1 kN/m^2, respectively. These results confirm that the strength of the unconsolidated samples decreases with (1) an increase in clay content and (2) an increase in the degree of alteration for samples affected by supergene (VoD3 and VoD4) or hydrothermal alteration (VoD5 and VoD6).

Eruption source conditions

The energy released during decompression, which drives the fragmentation and ejection of particles, is controlled, in this phreatic case, by the amount of water in the system. Thus porosity and sample water content are the main parameters affecting the ejection dynamics of particles during decompression (Mayer et al. 2015).

We observed a non-linear decay of the ejection velocity as a function of time irrespective of the particle size, sample porosity, and water content (Fig. 8). Grouping particles by size into lapilli (> 2 mm) and ash (< 2 mm) revealed the following results:

(1) Independent of the experiment conditions (3 bar/115 °C or 5 bar/125 °C), the first ejected particles were smaller than 500 μm and exhibited the highest ejection speeds (55–70 m/s), which is in agreement with previous studies at Stromboli (e.g., Harris et al. 2012a, b).

Table 1 Mineral composition and major and trace element analyses for investigated samples affected by supergene and hydrothermal alteration

	Supergene alteration				Hydroth. alt.	
	VoD1	VoD2	VoD3	VoD4	VoD5	VoD6
Mineral phases (determined by X-ray powder diffraction)						
Plagioclase	37 ± 3	32 ± 3	16 ± 3	18 ± 3		
Sanidine	15 ± 2	12 ± 2	8 ± 2			
Hornblende	2 ± 1					
Clinopyroxene				2 ± 1		
Cristobalite	20 ± 2	23 ± 2	8 ± 2	6 ± 2	15 ± 2	13 ± 2
Quartz	2 ± 1	2 ± 1	5 ± 1	1 ± 1	2 ± 1	4 ± 1
Pyrite	1 ± 1	1 ± 1	3 ± 1			
Alunite[a]					25 ± 3	47 ± 3
Montmorillonite	23 ± 2	30 ± 3	60 ± 3	73 ± 3		
Kaolinite					58 ± 3	36 ± 3
Sum	100	100	100	100	100	100
Major elements (%)[b]						
SiO_2	61.5	65.1	59.2	54.8	54.5	49.8
TiO_2	0.5	0.6	0.6	1.0	0.6	0.5
Al_2O_3	17.0	17.5	17.5	20.2	19.2	13.5
Fe_2O_3	5.8	3.7	6.3	7.9	3.9	2.9
MnO	0.1	0.1	0.1	0.1	0.1	0.1
MgO	1.6	0.9	1.7	3.6	0.7	0.9
CaO	5.2	3.7	3.5	3.4	0.7	2.7
Na_2O	3.0	2.8	1.5	1.4	1.0	2.1
K_2O	1.6	1.7	1.1	0.2	1.4	1.2
P_2O_5	0.1	0.1	0.1	0.1	0.1	0.2
SO_3	0.7	0.3	0.6	0.4	10.7	10.7
LOI	3.4	2.9	9.3	6.8	17.6	26.4
Sum	99.8	98.9	99.4	99.8	99.7	100.0
Trace elements (ppm)[b]						
Ba	267	266	220	115	0	544
Cr	< 20	< 20	< 20	128	< 20	< 20
Cu	48	82	71	< 30	117	92
Ni	7	1	< 20	< 20	70	50
Rb	53	55	31	< 30	48	40
Sr	192	161	102	90	192	133
Y	40	30	21	17	0	0
Zn	90	46	99	96	52	59
Zr	103	103	113	77	87	74

[a] Includes Na- and K-dominated alunites

[b] Determined by wavelength dispersive X-ray fluorescence

(2) Lapilli-sized particles (> 2 mm) occurred at a later stage of the ejection (after 12.5 ms) and had slower ejection velocities (25–50 m/s); this also confirms natural data from Stromboli (e.g., Taddeucci et al. 2012).
(3) As initial pressure and temperature were increased, at-source ejection velocities increased from 40–50 m/s to 65–80 m/s for the ash and lapilli of sample VoD5 and from 25–40 m/s to 55–70 m/s for VoD6.
(4) VoD5 had higher ejection velocities (40–80 m/s) than VoD6 (25–70 m/s), which was associated with a higher water content in VoD5 (67.3%) than in VoD6 (49.9%).
(5) Calculated trajectory distances for VoD5 (22–65 m) were higher than for VoD6 (21–40 m).
(6) For both samples, distance increased with particle size, ranging from 21 to 24 m for ash and 35–65 m for lapilli.

These results are in good agreement with studies of hydrothermal explosions occurring in Iceland and involving the ejection of unconsolidated and hydrothermally altered material of similar grain size (Montanaro et al. 2016).

Discussion

Hydrothermal activity

The spatial distribution of hydrothermal features in the VoD is likely controlled by the structural setting (Schöpa et al. 2011), as also proposed by Traineau et al. (2015) for the Boiling Lake area. Nevertheless, the intensity and style of hydrothermal activity, including the phreatic eruptions, seem to be influenced by alteration processes at the surface and at shallow depth. As our results show, rock/soil permeability is a major parameter because degassing is significantly changed (reduced by over two orders of magnitude; see Table 3) by alteration processes present in the VoD.

By comparing our mapping results with the descriptions made after the phreatic eruption of 1880 (Sapper 1903) and the report of James (1997) following the 1997 eruption, the following inferences can be made:

(1) Advanced argillic alteration affecting mainly the area close to hydrothermal vents results in the formation of a clay-rich material, which exhibits a lower strength and is generally more easily eroded than surrounding consolidated rocks (Figueiredo et al. 1999). Thus, gullies and rills mostly develop in areas where fumaroles, hot springs, and bubbling pools are located.
(2) Despite the constant modification to topography in the VoD due to denudation and mass-movement, the main hydrothermal features (fumaroles and mud pools). remained at the same locations during the period 1880–2015 (Figs. 2 and 3). Such persistence of emission location has also been well-documented at Vulcano, where it results from the occurrence of deep-seated, structurally controlled

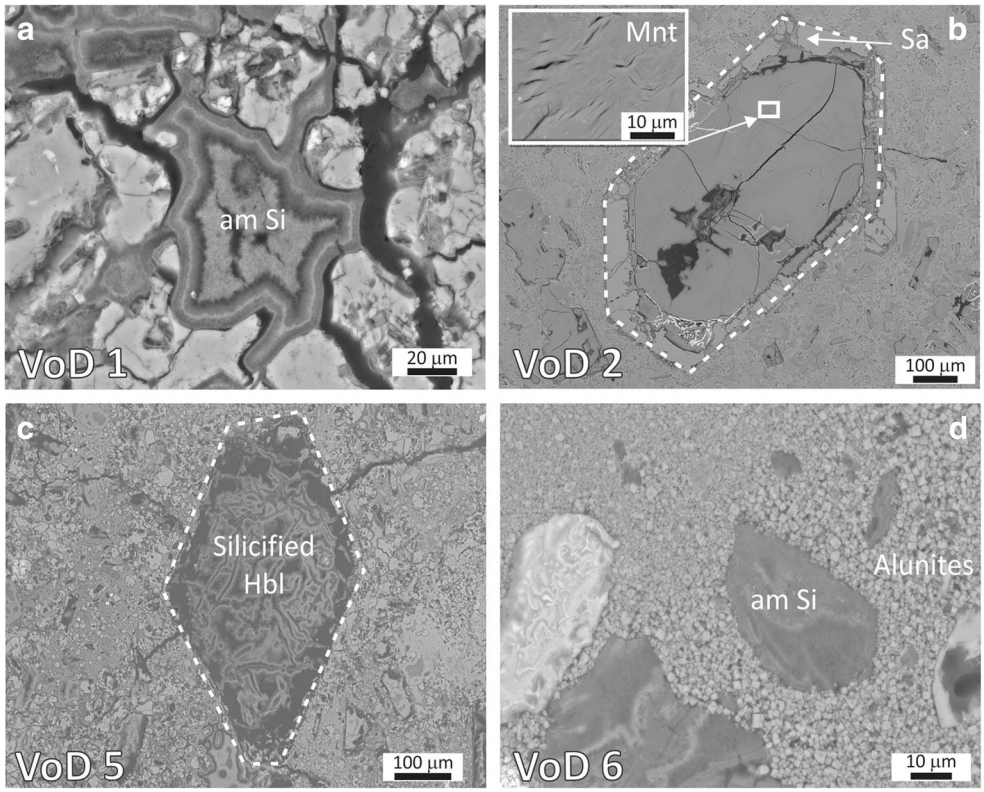

Fig. 7 BSE-SEM images of investigated samples. **a** Precipitates of amorphous silica (am Si) in pore space showing growth zonation. **b** Outline of a euhedral sanidine (dashed line) which has been replaced by montmorillonite. Remnants of sanidine (Sa) are in bright gray. The rectangle shows a zoom into the core area of the sanidine which has been replaced by montmorillonite (Mnt). The zoomed inset highlights the layered structure of montmorillonite. **c** Amorphous silica pseudomorph after hornblende (Hbl) (~ 400 µm) within a fine-grained matrix. **d** Rectangular fragments (30–40 µm) of amorphous silica pseudomorphs within a fine-grained matrix consisting of euhedral alunite crystals (< 2 µm)

high-permeability pathways that surficial modifications do not effect (Harris and Maciejewski 2000).

(3) Although a significantly larger amount of material was ejected during the more energetic 1880 eruption (Watt 1880) compared to the 1997 phreatic eruption (Lindsay et al. 2005), it is still described as a phreatic eruption since there was no involvement of any juvenile material (Watt 1880). The crater which formed during the 1880 eruption was filled (to a certain extent) by its own ejecta (Watt 1880). Subsequent crater filling resulted from slumping processes and retrograde erosion of its crater walls (Nicholls 1880; Sapper 1903). Hydrothermal features located mainly along the margin of the oval crater-shaped valley could therefore be related to the discontinuity between the host rock and the loose reworked crater-filling material. Such a zone might facilitate the rise of fluids at shallow depth, as observed in studies from Vulcano, Campi Flegrei, and Nysiros (Harris and Maciejewski 2000; Iacono et al. 2009; Pantaleo and Walter 2014). Similar processes of fluid circulation along a discontinuity have been observed during flank collapse studies in the Lesser Antilles (Boudon et al. 2007) and elsewhere around the world (Waythomas 2012). Hydrothermal outflow at greater depth is most commonly associated with the structural setting (i.e., Curewitz and Karson 1997; Rowland and Sibson 2004), which is

Table 2 Averaged sample properties including petrophysical properties obtained during field and laboratory analysis

CIA[a]	PIA[b]	CIW[c]
63.6	65.5	67.6
68.1	70.8	72.9
80.3	76.6	77.8
80.2	80.6	80.8
86.1	91.3	91.9
69.5	72.2	74.0

[a] Chemical index of alteration $\frac{(Al_2O_3)\times 100}{(Al_2O_3+CaO+Na_2O+K_2O)}$ Nesbitt and Young (1982)

[b] Plagioclase index of alteration (PIA) $\frac{(Al_2O_3-K_2O)\times 100}{(Al_2O_3+CaO+Na_2O-K_2O)}$ Fedo et al. (1995)

[c] Chemical index of weathering (CIW) $\frac{(Al_2O_3)\times 100}{(Al_2O_3+CaO+Na_2O)}$ Harnois (1988)

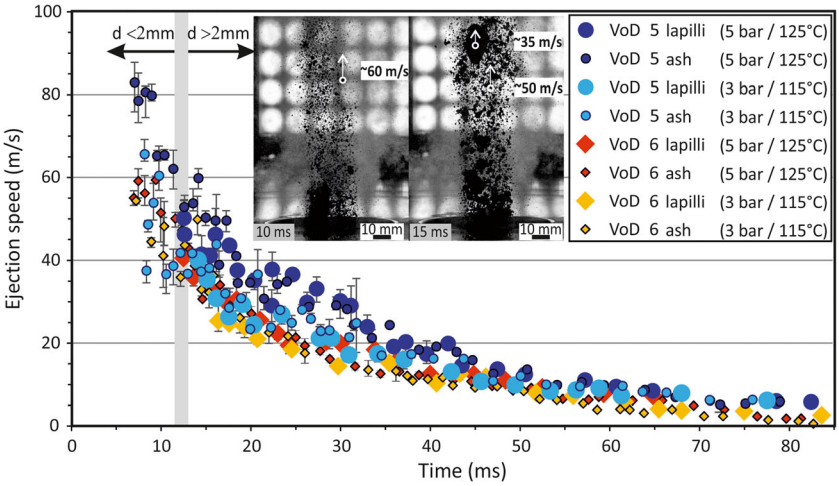

Fig. 8 Ejection speed of particles determined by analysis of high-speed camera footage of the rapid decompression experiments. The velocity of the particles decays with time. Coarser particles (d > 2 mm, with d = particle diameter) exhibit lower ejection speeds and appear in the field of view at a later stage of the ejection. Insets represent sequences of still-frames from high-speed camera recordings showing the ejection of particles at different times (10 ms, 15 ms) after the initiation of the decompression. The onset of the ejection is characterized by the expulsion of fine particles followed by a mixture of fine and coarse particles

thought to provide the pathways for the persistent activity in the VoD.

(4) The northern part of the VoD changed within approximately the last 100 years from intense fumarolic degassing (Sapper 1903) to mud pool activity (Figs. 2a and 3). Both hydrothermal and supergene alteration results in the formation of low permeability clay-rich layers. This in turn may lead to increased condensation of fluids at shallow depth, which could have induced a gradual change from emission of gaseous fluids as fumaroles to the development of bubbling mud pools within a shallow liquid-dominated zone (Fig. 4c, d). Such a change in activity might also be favored as this part of the VoD is located within a depression with little drainage. The mud pools occasionally show increased activity associated with burst events and minor mud jets, which eject hot mud up to several meters in distance.

Effects of hydrothermal alteration

Geochemical and mineralogical analysis of investigated samples revealed that two types of alteration are prominent in the VoD. Supergene argillic alteration of the host rocks leads to the formation of montmorillonite-rich unconsolidated material (Table 1). This alteration process led to the development of a clay-rich soil horizon at the surface. Advanced argillic alteration by acid-sulfate fluids affects the vent locations, causing leaching and complete decomposition of feldspars and hornblendes to kaolinite and alunite (Pirajno 2009). The VoD

Table 3 Chemical alteration indices of investigated samples

Sample	M (%)	Wc (%)	Cc (%)	ρB (g/cm^3)	ρM (g/cm^3)	φ (%)	k (m^2)	σ (kN/m^2)	τ (kN/m^2)
VoD1	n.m.	n.m.	23	2.22	2.61	14.8	2.5×10^{-15}[a]	n.m.	n.m.
VoD2	n.m.	n.m.	30	2.18	2.49	17.3	8.5×10^{-15}[a]	n.m.	n.m.
VoD3	34.9	26.3	52	1.74	2.58	50.2	3.6×10^{-15}[b]	> 5.0[d]	3.1
VoD4	41.5	32.1	73	1.58	2.76	65.5	2.1×10^{-14}[b]	0.9	1.6
VoD5	87.8	67.3	58	1.56	2.56	73.1	$< 5.6 \times 10^{-16}$[b,c]	1.4	0.8
VoD6	54.9	49.9	36	1.52	2.56	65.5	9.4×10^{-15}[b]	2.4	2.7

M moisture obtained with PL-300, *Wc* water content obtained by drying, *Cc* clay content, *ρB* bulk density, *ρM* matrix density, φ connected porosity, *k* gas permeability, σ uniaxial compressive strength (UCS), τ shear strength

[a] Gas permeability determined by benchtop permeameter under a confining pressure of 1 MPa

[b] In situ air permeability determined by PL-300 soil permeameter (Umwelt-Geräte-Technik)

[c] Sample permeability below measurement range of device

[d] Unconfined compressive strength (UCS) exceeded the range of the device (5.0 kN/m^2)

represents an example of how the presence of meteoric water influences the mineral zoning within an advanced argillic alteration sequence (i.e., Fulignati et al. 2002; Boyce et al. 2007). The highly water-saturated horizon (VoD5) in the lower part of the escarpment of the "Mini valley" (Fig. 5) is dominated by kaolinite (and lesser amounts of alunite), whereas the overlying, alunite-dominated layer (VoD6) has a lesser amount of kaolinite and is located above the water saturation level. The dominance of alunite over kaolinite in the upper part of the valley wall indicates that alunite formation is favored above the water table where atmospheric oxidation of H_2S to H_2SO_4 occurs (Mutlu et al. 2005).

Alteration indices can be applied to confirm (i) the degradation of rock petrophysical properties by alteration, (ii) the influence of supergene alteration, and (iii) the effect of hydrothermal alteration on rock mechanical properties (Table 2; Pola et al. 2012). Derived porosities, densities, and water contents are typical for those of clay-rich materials and agree well with the values of residual and volcanic soil investigated in other locations on Dominica and similar volcanic environments (Rouse et al. 1986; Rao 1996; Del Potro and Hürlimann 2009). Moreover, the increasing degree of alteration is reflected by decreasing rock strength—a relationship observed for samples affected by supergene and hydrothermal alteration in this study and elsewhere (Del Potro and Hürlimann 2009). The results confirm previous investigations, which showed that the formation of clay is associated with intense weakening leading to the destabilization of the rocks, which in turn causes landslides and collapse (Montalto 1994; Boudon et al. 2007).

Petrophysical properties of investigated unconsolidated samples show that altered rocks in a volcanic environment represent very weak units and that their behavior is furthermore controlled by particle size distribution and water content (Del Potro and Hürlimann 2008 and references therein). As our results show, clay alteration leads to decreasing permeability and thereby affects the degassing of hydrothermal active areas (Alvarado et al. 2010; Harris et al. 2012b). Surficial sulfur-rich encrustations, observed in the close vicinity of degassing vents (Fig. 3), could further contribute to a decrease in permeability and create sealing levels within surficial lithological units, as observed at Vulcano by Harris and Maciejewski (2000).

Permeability is a key factor in the pressurization events (Browne and Lawless 2001). In our investigated samples, permeability is mainly controlled by clay formation and precipitation of alunite. The hydrothermally altered zone, which is characterized by low permeability lithologies, is thus prone to pressurization, especially as the acidic fluids are emitted from this zone. The pressurization of the hydrothermal system could be caused by an increased fluid flux to the surface resulting from changes within the hydrothermal system (e.g., fracturing of sealed zones, inflow of meteoric fluids, rainfall, changes in the groundwater table). Such an increased fluid flux could also be caused by a rising flux of magmatic fluids. Pressurization could also be caused by constant gas flow but continuously decreasing permeability (due to clay formation and precipitation of secondary minerals). Following our results, the capping of degassing vents by low permeability layers blocked the pathways for fluid flow which led to pressurization. This is in agreement with the work by Chiodini et al. (1995) on Vulcano where sudden decompression of the shallow hydrothermal system, or entry of water into that system, during an earthquake is one potential eruption scenario. As the lithologies in the vicinity of degassing vents (VoD5–VoD6) are relative low strength, rupture and decompression might occur even at little overpressure. Such small-volume eruptions might further be favored by heavy rainfall (as is common during cyclones in tropical environments) which shocks the surficial hydrothermal system by a rapid fluid input increase. Along with the plugging of the system by a landslide, a pressure build-up with the potential for sudden decompression could be inevitable. Such a scenario and eruptive style might therefore be more likely in tropical environments.

Ejection behavior of altered unconsolidated material

Results obtained by rapid decompression experiments with heavily altered, clay-rich material at initial pressures of 0.3 and 0.5 MPa confirmed the influence of particle size on ejection speed. As most of the kinetic energy is released during the initial stage of decompression, and smaller particles are more efficiently coupled with the expanding gas and steam, ash-sized particles arriving during an early stage in the field of view exhibit the highest ejection velocities (Alatorre-Ibargüengoitia et al. 2010; Harris et al. 2012a).

Estimated trajectory distances (up to 65 m) correspond well with the reported maximum distances obtained by particles (52 m) ejected during the 1997 phreatic eruption (James 1997). The asymmetrical distribution of ejecta to the west, as described by James (1997), was most likely caused by a lateral jet (Table 4). However, information on the direction and speed of wind during the eruption period is lacking. Our conceptual model for the probable evolution of the 1997 phreatic eruption in the VoD is given in Fig. 9. Landslide deposits derived from slope failure at Morne Watt would have caused an uneven coverage of the degassing locations, which resulted in a lower overburden towards the valley side. This favored an expansion of fluids in this direction and caused a directed jet of steam and debris to the NW of the source location.

Summary and conclusions

Two field campaigns and laboratory analysis, in combination with a comprehensive literature review, allowed us to (1) gain

Table 4 Estimated trajectory distances based on ejection speeds obtained during decompression experiments by high-speed video analysis. For the calculation, the in situ bulk density was used and an ejection angle of 45° was assumed

Sample	Size	Pressure (MPa)	Temperature (°C)	V_{eject} [a] (m/s)	$Traj_{min}$ [b] (m)	$Traj_{max}$ [c] (m)
VoD5	Lapilli	0.5	125	50	20	65
VoD5	Ash	0.5	125	80	12	24
VoD5	Lapilli	0.3	115	40	18	56
VoD5	Ash	0.3	115	65	11	22
VoD6	Lapilli	0.5	125	40	17	40
VoD6	Ash	0.5	125	70	11	21
VoD6	Lapilli	0.3	115	25	13	35
VoD6	Ash	0.3	115	55	10	21

[a] Ejection speed of particles obtained by high-speed video analysis

[b] Minimum trajectory distance calculated with Eject! (Mastin 2001)

[c] Maximum trajectory distance calculated with Eject! (Mastin 2001)

further insight into the historical and most recent hydrothermal phreatic eruptions in the VoD and (2) investigate phreatic activity and alteration processes in the VoD. A detailed map of the VoD showing the distribution of hydrothermal occurrences and soils affected by alteration, as observed during fieldwork in 2013 and 2015, is presented. The map serves as a basis for further investigation of hydrothermal activity in the area, as it represents a snapshot of activity in an environment subjected to various surface processes which affect the degassing style and intensity. As at other sites characterized by hydrothermal activity, the locations of degassing sources are constantly changing so that repeat surveys are justified to track the temporal and spatial evolutions of the emissions (e.g., Harris et al. 2012a).

Field and laboratory-based characterization, including in situ permeability measurements of altered unconsolidated rocks, revealed several characteristics of supergene and hydrothermal alteration in an active hydrothermal area:

(1) Rocks within the VoD are generally affected by intermediate supergene argillic alteration, causing disaggregation and the formation of montmorillonite.
(2) The close proximity of degassing vents is characterized by advanced argillic alteration and the formation of kaolinite and alunite.
(3) Both types of alteration decreased rock strength and permeability and were accompanied by an increasing abundance of clay minerals.
(4) Advanced argillic alteration in the vicinity of degassing vents (causing clay formation and a decrease in permeability) may have enhanced condensation of fluids at shallow depth, therefore inducing the progressive change

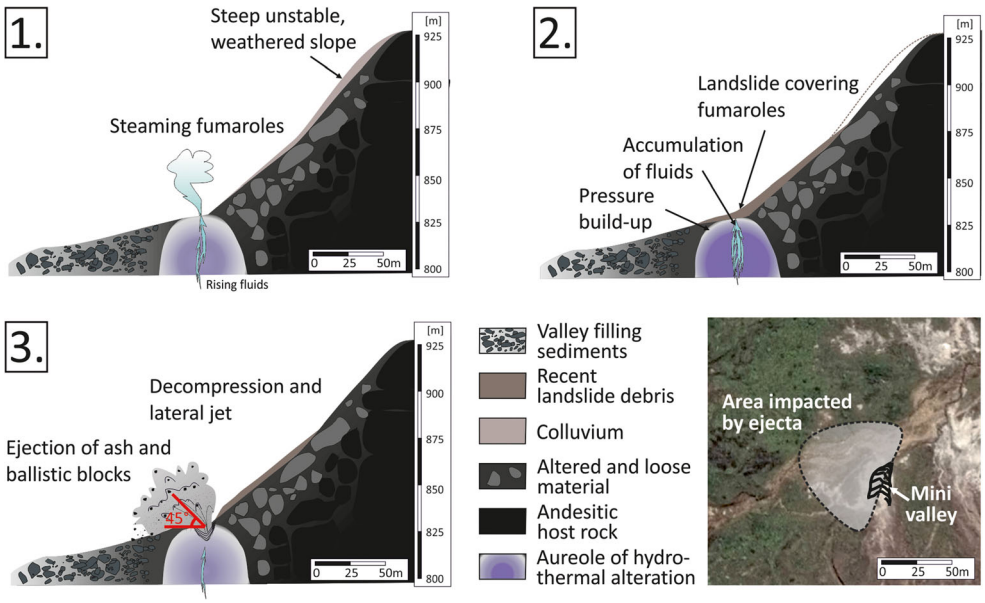

Fig. 9 Conceptual model showing a possible scenario for the evolution of the 1997 phreatic eruption in the Valley of Desolation. The landslide deposits might have caused an uneven coverage of the vent locations, which most likely resulted in an overpressure build-up and a lateral jet of steam and particles. The distribution of the ejecta was thus dominantly in an area to the NW of the source location, as reported by a field investigation (James 1997)

from steaming fumaroles to boiling mud pools.

(5) Strength reduction of altered rock/soil could have caused destabilization in steeply sloping areas, which may have increased the occurrence of landslides. These covered pre-existing fluid-emitting vents, thus hindering degassing, which led to pressurization (a similar process most probably triggered the 1997 phreatic eruption in the VoD).

Our results furthermore demonstrate that the degradation of physical rock properties, induced by supergene and hydrothermal alteration, is well reflected in chemical alteration indices (i.e., CIA, PIA, and CIW).

In addition, decompression experiments and analytical modeling on hydrothermally altered samples made it possible to reconstruct the dynamics of the 1997 phreatic event in the VoD and to estimate the conditions (3–5 bar; 115–125 °C) leading to such events. Based on observations of the 1997 eruption and the experimental results, a conceptual model for the progression of the events which occur during a landslide-triggered phreatic eruption in the VoD has been provided. Landslides thus represent a potential trigger mechanism for volcanic activity in geothermal areas (Hansell et al. 2006). Furthermore, sudden fluid input increase during extreme rainfall probably contributes to the potential triggering of such a scenario (Martini et al. 1981, Marini et al. 1993) and should therefore be investigated in the future.

Our findings shed light on the processes of hydrothermal alteration associated with landslide-triggered phreatic eruptions. New techniques for mapping and monitoring of alteration processes, which induce mechanical instability of degassing vent-systems, must be developed for all the active volcanoes of the Lesser Antilles (Boudon et al. 2007) and elsewhere. The results presented in this study may therefore be considered as a contribution to such efforts at the VoD and at similar hydrothermally active environments.

Acknowledgements This project has received funding from the European Union's Seventh Program for research, technological development, and demonstration under grant agreement no. 282759 (VUELCO). C. Montanaro and B. Scheu acknowledge the support of the European Commission (FP7-MCITN, grant no. 289976: NEMOH). C. Montanaro, B. Scheu, and D.B. Dingwell acknowledge the support from EC FP7 grant agreement no. 308665 (MED-SUV). K. Mayer acknowledges S. Wiesmaier, D. Morgavi, L. Spina, D. Robertson, and S. Müller for the help during the sampling. K. Mayer thanks the Division of Forestry, Wildlife and National Parks of Dominica for the sampling permission. K. Mayer also acknowledges Jeffrey and J. Arlington for the fruitful discussions and personal reports on activity in the study area. K. Mayer acknowledges C. Cimarelli for acquiring images with the FE-SEM (Hitachi SU5000) at the Key Facility Analytische Raster-Elektronenmikroskopie of the Department for Earth and Environmental Sciences of the LMU. K. Mayer and D.B. Dingwell acknowledge the support of the ERC Advanced Investigator Grant (EVOKES—no. 247076). We thank Isabelle Chambefort, Natalia Pardo, Pierre-Simon Ross, Andrew Harris, and an anonymous reviewer for their comments which significantly improved this manuscript.

References

Alatorre-Ibargüengoitia MA, Scheu B, Dingwell DB, Delgado-Granados H, Taddeucci J (2010) Energy consumption by magmatic fragmentation and pyroclast ejection during Vulcanian eruptions. Earth Planet Sci Lett 291:60–69

Alvarado GE, Carboni S, Cordero M, Avilés E, Valverde M (2010) Stability of the cone and foundation of Arenal Volcano, Costa Rica. In Volcanic rock mechanics. Balkema Leiden, The Netherlands, pp 159–166

Arıkan F, Ulusay R, Aydın N (2007) Characterization of weathered acidic volcanic rocks and a weathering classification based on a rating system. Bull Eng Geol Environ 66:415–430

Bergmann J, Friedel P, Kleeberg R (1998) BGMN—a new fundamental parameters based Rietveld program for laboratory X-ray sources, its use in quantitative analysis and structure investigations. CPD Newsl 20:5–8

Boudon G, Le Friant A, Komorowski JC, Deplus C, Semet MP (2007) Volcano flank instability in the Lesser Antilles Arc: diversity of scale, processes, and temporal recurrence. J Geophys Res Solid Earth 112

Boyce AJ, Fulignati P, Sbrana A, Fallick AE (2007) Fluids in early stage hydrothermal alteration of high-sulfidation epithermal systems: a view from the Vulcano active hydrothermal system (Aeolian Island, Italy). J Volcanol Geotherm Res 166(2):76–90

Browne PRL, Lawless JV (2001) Characteristics of hydrothermal eruptions, with examples from New Zealand and elsewhere. Earth Sci Rev 52:299–331

Chiodini G, Cioni R, Marini L, Panichi C (1995) Origin of the fumarolic fluids of Vulcano Island, Italy, and implication for volcanic surveillance. Bull Volcanol 57:99–110

Curewitz D, Karson JA (1997) Structural settings of hydrothermal outflow: fracture permeability maintained by fault propagation and interaction. J Volcanol Geotherm Res 79:149–168

Del Potro R, Hürlimann M (2008) Geotechnical classification and characterization of materials for stability analyses of large volcanic slopes. Eng Geol 98:1–17

Del Potro R, Hürlimann M (2009) The decrease in the shear strength of volcanic materials with argillic hydrothermal alteration, insights from the summit region of Teide stratovolcano, Tenerife. Eng Geol 104(1):135–143

Demange J, Iundt F, Puvilland P (1985) Geothermal field model of Wotten Waven Island of Dominica Lesser Antilles. Geothermal Resour Council Trans 9:409–415

Di Napoli R, Aiuppa A, Allard P (2014) First multi-gas based characterization of the Boiling Lake volcanic gas (Dominica, Lesser Antilles). Ann Geophys 56:S0559

Duzgoren-Aydin NS, Aydin A, Malpas J (2002) Re-assessment of chemical weathering indices: case study on pyroclastic rocks of Hong Kong. Eng Geol 63:99–119

Endlich FM (1880) The island of Dominica. Am Nat 14:761–772

Farquhar G (2001) Guideline for hand held shear vane test. New Zealand Geotechnical Society

Fedo CM, Wayne NH., and Young GM. (1995) "Unraveling the effects of potassium metasomatism in sedimentary rocks and paleosols, with implications for paleoweathering conditions and provenance." Geology 23. 10:921-924.

Figueiredo MDA, Augustin CHRR, Fabris JD (1999) Mineralogy, size, morphology and porosity of aggregates and their relationship with

soil susceptibility to water erosion. Hyperfine Interactions 122:177–184

Fournier N, Witham F, Moreau-Fournier M, Bardou L (2009) Boiling Lake of Dominica, West Indies: high-temperature volcanic crater lake dynamics. J Geophys Res Solid Earth 114(B2)

Fulignati P, Sbrana A, Luperini W, Greco V (2002) Formation of rock coatings induced by the acid fumarole plume of the passively degassing volcano of La Fossa (Vulcano Island, Italy). J Volcanol Geotherm Res 115(3):397–410

Glasmann JR (1982) Alteration of andesite in wet, unstable soils of Oregon's western Cascades. Clay Clay Miner 30:253–263

Gurioli L, Zanella E, Gioncada A, Sbrana A (2012) The historic magmatic-hydrothermal eruption of the Breccia di Commenda, Vulcano, Italy. Bull Volcanol 74(5):1235–1254

Hansell AL, Horwell CJ, Oppenheimer C (2006) The health hazards of volcanoes and geothermal areas. Occup Environ Med:149–156

Harnois L (1988) "The CIW index: a new chemical index of weathering." Sedimentary Geology 55.3-4 :319-322.

Harris AJL, Maciejewski AJH (2000) Thermal surveys of the Vulcano Fossa fumarole field 1994–1999: evidence for fumarole migration and sealing. J Volcanol Geotherm Res 102:119–147

Harris A, Alparone S, Bonforte A, Dehn J, Gambino S, Lodato L, Spampinato L (2012a) Vent temperature trends at the Vulcano Fossa fumarole field: the role of permeability. Bull Volcanol 74(6): 1293–1311

Harris AJ, Ripepe M, Hughes EA (2012b) Detailed analysis of particle launch velocities, size distributions and gas densities during normal explosions at Stromboli. J Volcanol Geotherm Res 231:109–131

Heap MJ, Kennedy BM, Farquharson JI, Ashworth J, Mayer K, Letham-Brake M, Reuschle T, Gilg HA, Scheu B, Lavallee Y, Siratovich P, Cole J, Jolly AD, Baud P, Dingwell DB (2017) A multidisciplinary approach to quantify the permeability of the Whakaari/White Island volcanic hydrothermal system (Taupo Volcanic Zone, New Zealand). J Volcanol Geotherm Res 332:88–108

Iacono DD, Zollo A, Vassallo M, Vanorio T, Judenherc S (2009) Seismic images and rock properties of the very shallow structure of Campi Flegrei caldera (southern Italy). Bull Volcanol 71(3):275–284

James A (1997) Observations made in the Valley of Desolation following a volcanic eruption, July 1997. Unpublished report, Forestry and Wildlife Division, Dominica

Joseph EP, Fournier N, Lindsay JM, Fischer TP (2011) Gas and water geochemistry of geothermal systems in Dominica, Lesser Antilles island arc. J Volcanol Geotherm Res 206:1–14

Lindsay JM, Stasiuk MV, Shepherd JB (2003) Geological history and potential hazards of the Late-Pleistocene to Recent Plat Pays volcanic complex, Dominica, Lesser Antilles. Bull Volcanol 65:201–220

Lindsay JM, Smith AL, Roobol MJ, Stasiuk MV (2005) Dominica. In: Lindsay JM, Robertson REA, Shepherd JB, Ali S (eds) Volcanic Hazard Atlas of the Lesser Antilles-Seismic Research Unit. The University of the West Indies, Trinidad and Tobago, pp 1–48

Makó A, Elek B, Dunai A, Hernadi H (2009) Comparison of nonaqueous phase liquids' conductivity and air permeability of different soils. Commun Soil Sci Plant Anal 40:787–799

Marini L, Principe C, Chiodini G, Cioni R, Fytikas M, Marinelli G (1993) Hydrothermal eruptions of Nisyros (Dodecanese Greece). Past events and present hazard. J Volcanol Geotherm Res 56:71–94

Martini M, Piccardi G, Cellini Legittimo P (1981) The effect of variations in rainfall on the chemical composition of Vulcano fumaroles (Italy). Bull Volcanol 44:110–113

Mastin LG (1995) Thermodynamics of gas and steam-blast eruptions. Bull Volcanol 57:85–98

Mastin LG (2001) A simple calculator of ballistic trajectories for blocks ejected during volcanic eruptions: U.S. Geological Survey Open-File Report 01–45, 16p

Mayer K, Scheu B, Gilg HA, Heap M, Kennedy BM, Lavallée Y, Letham-Brake M, Dingwell DB (2015) Experimental constraints on phreatic eruption processes at Whakaari (White Island volcano). J Volcanol Geotherm Res 302:150–162

Mayer K, Scheu B, Montanaro C, Yilmaz TI, Isaia R, Aßbichler D, Dingwell DB (2016) Hydrothermal alteration of surficial rocks at Solfatara (Campi Flegrei): petrophysical properties and implications for phreatic eruption processes. J Volcanol Geotherm Res 320:128–143

Montalto A (1994) Seismic signals in geothermal areas of active volcanism: a case study from 'La Fossa', Vulcano (Italy). Bull Volcanol 56(3):220–227

Montanaro C, Scheu B, Gudmundsson MT, Vogfjörd K, Reynolds HI, Dürig T, Strehlow K, Rott S, Reuschlé T, Dingwell DB (2016) Multidisciplinary constraints of hydrothermal explosions based on the 2013 Gengissig lake events, Kverkfjöll volcano, Iceland. Earth Planet Sci Lett 434:308–319

Mutlu H, Sariiz K, Kadir S (2005) Geochemistry and origin of the Şaphane alunite deposit, Western Anatolia, Turkey. Ore Geol Rev 26:39–50

Nesbitt HW, Young GM (1982) "Early Proterozoic climates and plate motions inferred from major element chemistry of lutites." Nature 299.5885 (1982): 715-717.

Nicholls HAA (1880) The volcanic eruption in Dominica. Nature 21: 372–373

Pirajno F (2009) Hydrothermal processes and mineral systems. Springer Netherlands, Dordrecht 1250 pages

Pantaleo M, Walter TR (2014) "The ring-shaped thermal field of Stefanos crater, Nisyros Island: a conceptual model." Solid Earth 5.1 183.

Pola A, Crosta G, Fusi N, Barberini V, Norini G (2012) Influence of alteration on physical properties of volcanic rocks. Tectonophysics 566:67–86

Rad S, Rivé K, Vittecoq B, Cerdan O, Allègre CJ (2013). Chemical weathering and erosion rates in the Lesser Antilles: An overview in Guadeloupe, Martinique and Dominica. Journal of South American Earth Sciences, 45:331-344.

Rao SM (1996) Role of apparent cohesion in the stability of Dominician allophane soil slopes. Eng Geol 43:265–279

Robson GR, Willmore PL (1955) Some heat measurements in West Indian soufrieres. Bull Volcanol 17:13–39

Roobol MJ, Smith AL (2004) Geological map of Dominica, West Indies. University of Puerto Rico at Mayaquez, Geology Department

Rouse WC, Reading AJ, Walsh RPD (1986) Volcanic soil properties in Dominica, West Indies. Eng Geol 23:1–28

Rowland JV, Sibson RH (2004) Structural controls on hydrothermal flow in a segmented rift system, Taupo Volcanic Zone, New Zealand. Geofluids 4(4):259–283

Sapper K (1903) Ein Besuch von Dominica. Zentralblatt für Mineralogie, Geologie und Paläontolgie, pp 305–314

Schöpa A, Pantaleo M, Walter TA (2011) Scale-dependent location of hydrothermal vents: stress field models and infrared field observations of the Fossa Cone, Vulcano Island, Italy. J Volcanol Geotherm Res 203:133–145

Smith AL, Roobol MJ, Mattioli GS, Fryxell JE, Daly GE, Fernandez LA (2013) The volcanic geology of the mid-arc Island of Dominica (Vol. 496). Geological Society of America

Taddeucci J, Scarlato P, Capponi A, Del Bello E, Cimarelli C, Palladino DM, Kueppers U (2012) High-speed imaging of strombolian explosions: the ejection velocity of pyroclasts. Geophys Res Lett 39(2)

Traineau H, Lasne E, Coppo N, Baltassa JM (2015) Recent geological, geochemical and geophysical surveys of the Roseau Valley, high-temperature geothermal field in Dominica, West Indies. Proceedings World Geothermal Congress 2015 Melbourne, Australia. 19–25 April 2015

Umwelt-Geräte-Technik (2012) PL-300 User's manual. Version18.03.2014. Müncheberg. www.ugt-online.de/fileadmin/media/products/01%20bodenkunde/downloads/PL-300/PL_300_en_Ver02.pdf

Wadsworth ME (1880) The volcanic dust from Dominica. Nature, July 22 1880, pp 266-267

Watt E (1880) The recent volcanic eruption in Dominica. Nature 22:77

Waythomas CF (2012) Landslides: landslides at stratovolcanoes initiated by volcanic unrest. In: Clague JJ, Stead D (eds) Landslides: types, mechanisms and modeling. Cambridge University Press, Cambridge

Worldbank (2017) https://data.worldbank.org/indicator/ST.INT.ARVL?locations=DM&view=map. Accessed 21 August 2017

Zimbone SM, Vickers A, Morgan RPC, Vella P (1996) Field investigations of different techniques for measuring surface soil shear strength. Soil Technol 9:101–111

http://data.worldbank.org/indicator/ST.INT.ARVL?locations=DM